August 13, 2018

A Deficit of Dark Matter from Jeans Modeling of the Ultra-diffuse Galaxy NGC 1052-DF2

Asher Wasserman, *University of California, Santa Cruz*
Aaron J. Romanowsky, *San Jose State University*
Jean Brodie, *University of California, Santa Cruz*
Pieter van Dokkum, *Yale University*
Charlie Conroy, *Harvard University*, et al.

The Astrophysical Journal Letters, 863:L15 (6pp), 2018 August 20 https://doi.org/10.3847/2041-8213/aad779

A Deficit of Dark Matter from Jeans Modeling of the Ultra-diffuse Galaxy NGC 1052-DF2

Asher Wasserman[1], Aaron J. Romanowsky[2,3], Jean Brodie[1,3], Pieter van Dokkum[4], Charlie Conroy[5], Roberto Abraham[6], Yotam Cohen[4], and Shany Danieli[4]
[1] Department of Astronomy & Astrophysics, University of California-Santa Cruz, Santa Cruz, CA 95064, USA; adwasser@ucsc.edu
[2] Department of Physics & Astronomy, San José State University, One Washington Square, San Jose, CA 95192, USA
[3] University of California Observatories, 1156 High Street, Santa Cruz, CA 95064, USA
[4] Astronomy Department, Yale University, New Haven, CT 06511, USA
[5] Department of Astronomy, Harvard University, Cambridge, MA 02138, USA
[6] Department of Astronomy & Astrophysics, University of Toronto, 50 St. George Street, Toronto, ON M5S 3H4, Canada
Received 2018 June 22; revised 2018 July 31; accepted 2018 July 31; published 2018 August 13

Abstract

The discovery of the ultra-diffuse galaxy NGC 1052-DF2 and its peculiar population of star clusters has raised new questions about the connections between galaxies and dark matter (DM) halos at the extremes of galaxy formation. In light of debates over the measured velocity dispersion of its star clusters and the associated mass estimate, we constrain mass models of DF2 using its observed kinematics with a range of priors on the halo mass. Models in which the galaxy obeys a standard stellar-halo mass relation are in tension with the data and also require a large central density core. Better fits are obtained when the halo mass is left free, even after accounting for increased model complexity. The dynamical mass-to-light ratio for our model with a weak prior on the halo mass is $1.7^{+0.7}_{-0.5}\ M_{\odot}/L_{\odot,V}$, consistent with the stellar population estimate for DF2. We use tidal analysis to find that the low-mass models are consistent with the undisturbed isophotes of DF2. Finally, we compare with Local Group dwarf galaxies and demonstrate that DF2 is an outlier in both its spatial extent and its relative DM deficit.

Key words: galaxies: halos – galaxies: individual (NGC 1052, DF2) – galaxies: kinematics and dynamics

1. Introduction

Ultra-diffuse galaxies (UDGs) were recently recognized as a ubiquitous class of low-surface-brightness stellar systems with luminosities like dwarf galaxies but sizes like giants (van Dokkum et al. 2015; Yagi et al. 2016). They are found in all environments from clusters and groups to the field (e.g., Martínez-Delgado et al. 2016; van der Burg et al. 2017), and appear to originate from multiple formation channels, including an extension of normal dwarfs to lower surface brightness, as tidal debris, and perhaps as "failed" galaxies (e.g., Peng & Lim 2016; Greco et al. 2018; Pandya et al. 2018).

The failed-galaxy scenario was motivated partly by inferences of UDG halo masses based on dynamics and on number counts of globular star clusters—masses that in some cases appear significantly higher than for the overall dwarf-galaxy population (Beasley et al. 2016; van Dokkum et al. 2016, 2017; Amorisco et al. 2018; Lim et al. 2018). The implication is that the stellar-to-halo mass relation (SHMR; e.g., Moster et al. 2013; Rodríguez-Puebla et al. 2017) for luminous dwarf galaxies ($L \sim 10^8\ L_{\odot}$) may have a much larger scatter than was presumed, requiring revisions in galaxy formation models at halo masses of $\sim 10^{11}\ M_{\odot}$ (see also Smercina et al. 2018).

In this context, one of the nearest known UDGs, NGC 1052-DF2 in a galaxy group at ~ 20 Mpc (Fosbury et al. 1978; Karachentsev et al. 2000; van Dokkum et al. 2018c, hereafter vD+18a), presents a valuable opportunity for detailed dynamical study. vD+18a used deep Keck spectroscopy to measure radial velocities for 10 luminous star clusters around DF2, estimating its dynamical mass within a radius of ~ 8 kpc (cf. Virgo-UDGs work by Beasley et al. 2016; Toloba et al. 2018). The result was very surprising: rather than an unusually *high* mass-to-light ratio (M/L) as found for previous UDGs, the M/L was unusually *low*, and consistent with harboring no dark matter (DM) at all.

The low/no-DM result generated spirited debate, much of which focused on how best to estimate the intrinsic velocity dispersion σ of DF2 (e.g., Laporte et al. 2018; Martin et al. 2018; van Dokkum et al. 2018a).

However, the more fundamental question is what range of halo mass profiles is permitted by the data, which we examine in detail in this Letter. We adopt a generative modeling approach where the individual velocity measurements are mapped statistically onto halo parameter space, without the intervening steps of estimating σ and applying a mass estimator. In addition to deriving constraints on the dynamical mass profile, we consider the potential impact of tidal stripping, and furthermore compare DF2 with Local Group (LG) dwarfs.

2. Observational Constraints

NGC 1052-DF2 has position, redshift, surface brightness fluctuation (SBF), and tip of the red giant branch measurements that are all consistent with being a satellite of the giant elliptical galaxy NGC 1052 (vD+18a; van Dokkum et al. 2018d). We adopt a distance of 19 Mpc, matching the measured SBF distance to DF2 (Cohen et al. 2018), while allowing for a ± 1 Mpc uncertainty in our analysis.[7]

The UDG surface brightness follows a Sérsic profile with index $n = 0.6$, effective radius $R_e = 22.''6$ (2.08 kpc), and total luminosity of $1.2 \times 10^8\ L_{V,\odot}$. For the stellar M/L, we adopt a Gaussian prior with mean of $\Upsilon_{*,V} = 1.7$ in Solar units and standard deviation of 0.5 (based on stellar population

[7] A distance of 13 Mpc has been proposed (Trujillo et al. 2018), but see van Dokkum et al. (2018d) for an in-depth discussion of the evidence for the greater distance.

modeling; vD+18a; van Dokkum et al. 2018b). We truncate this distribution to be between 0.1 and 10.

NGC 1052-DF2 has 10 star clusters with radial velocity measurements in vD+18a. We use one updated velocity from van Dokkum et al. (2018a); this has only a mild impact on the results. Although the mass uncertainties from using so few tracers are relatively large (as we will find here), there is ample precedent in the literature for drawing meaningful conclusions from small sample sizes (Aaronson 1983; Chapman et al. 2005; Kleyna et al. 2005; Brown et al. 2007; Koposov et al. 2015).

The surface-density distribution of the star-cluster population is highly unconstrained. We assume an exponential distribution of tracers (i.e., a Sérsic profile with $n = 1$) where the half-number radius is drawn from a Gaussian prior with a mean of the observed half-number radius (32″) and standard deviation of 10″. We truncate this distribution to be between 10″ and 70″. Our adopted mean half-number radius is 40% larger than R_e of the galaxy diffuse starlight, which is consistent with studies of the star-cluster systems of other UDGs (Peng & Lim 2016; van Dokkum et al. 2017; Toloba et al. 2018; cf. Forbes 2017).

3. Jeans Modeling Methods

We use the Bayesian Jeans modeling formalism of Wasserman et al. (2018) to infer the mass distribution of DF2. Here, a given mass profile and a tracer density profile are linked to a predicted line-of-sight velocity dispersion profile $\sigma_J(R)$. The assumptions include spherical symmetry, dynamical equilibrium, and velocity-dispersion anisotropy ($\beta = 1 - \sigma_t^2/\sigma_r^2$) that is constant with galactocentric radius. (There is no evidence for rotation in the system, although individual velocity uncertainties are too large for strong constraints; vD+18a). We adopt a Gaussian prior on $\tilde{\beta} = -\log_{10}(1 - \beta)$ with a mean of 0 (isotropic) and standard deviation of 0.5 (truncated to the range of $\tilde{\beta} = -1$ to $+1$).

Because we do not directly constrain the dynamical mass beyond ∼8 kpc, we must rely on priors on the halo characteristics—on the DM profile shape, and also on expected correlations between halo mass, concentration, and stellar mass.

We model the mass distribution as the sum of the stellar mass, with spatial distribution described in Section 2, and a DM halo. For the halo density distribution we use the generalized Navarro–Frenk–White (gNFW) profile,

$$\rho(r) = \rho_s \left(\frac{r}{r_s}\right)^{-\gamma} \left(1 + \frac{r}{r_s}\right)^{\gamma - 3} \quad (1)$$

where r_s is the scale radius, ρ_s is the scale density, and γ quantifies the inner log-slope. For $\gamma = 1$, this matches the usual Navarro–Frenk–White (NFW) halo model (Navarro et al. 1997), but letting γ vary below 1 allows for models that have a cored, shallower density profile.

We re-parameterize the halo in terms of virial mass (M_{200c}) and concentration (c_{200c}), where

$$M_{200c} = 200 \rho_{crit} \frac{4\pi r_{200c}^3}{3} \quad (2)$$

and $c_{200c} = r_{200c}/r_s$.

We then consider two flavors of mass models: one in which the stellar and halo masses are drawn from a SHMR, and one where the stellar and dark masses are decoupled. For the latter model, we use a uniform prior on $\log_{10} M_{200c}/M_\odot$ between 2 and 15. This effectively allows for the case of no DM, as the stellar mass is $\log_{10} M_*/M_\odot \sim 8.3$.

For both types of models we assume that the halo concentration is drawn from a mass–concentration relation (MCR; Diemer & Kravtsov 2015; Diemer 2017) based on the *Planck 2015* cosmology. We use a log-normal distribution about this expected concentration with a scatter of 0.16 dex.

For the SHMR we use the $z = 0$ relation of Rodríguez-Puebla et al. (2017), where halos with mass $M_{200c} \sim 10^{10.8} M_\odot$ host galaxies with M_* similar to DF2 (note that for a satellite galaxy such as DF2, the halo mass is pre-infall, before tidal stripping). We allow for variation around this mean relation through a variable scatter:

$$\sigma_{\log M_*} = 0.2 - 0.26(\log M_{vir} - \log M_1) \quad (3)$$

below virial masses of $M_1 = 10^{11.5} M_\odot$ (note $M_{vir} \neq M_{200c}$; at M_1, $M_{200c} \sim 0.9 M_{vir}$), while at higher masses, $\sigma_{\log M_*}$ is a constant 0.2 dex scatter (Garrison-Kimmel et al. 2017; Munshi et al. 2017).

Given the wide range of possible baryonic effects on the inner slope of DM halos (Oh et al. 2011; Adams et al. 2014; Pineda et al. 2017), we adopt a uniform prior on γ between 0 and 2.

To connect the Jeans model predictions for σ_J to the velocity observations, we use a Gaussian likelihood for the probability of drawing data, v_i, given the location R_i and the various model parameters θ,

$$\begin{aligned} \mathcal{L}(v_i|R, \theta) &= \mathcal{N}(v_i - v_{sys}, \sigma^2 = \sigma_J^2(R|\theta) + \delta v_i^2) \\ &= (2\pi\sigma^2)^{-1/2} \exp\left(-\frac{(v_i - v_{sys})^2}{\sigma^2}\right) \end{aligned} \quad (4)$$

where v_{sys} is the systemic velocity (drawn from a Gaussian prior with a mean of the observed velocities, 1801.6 km s^{-1}, and with a 5 km s^{-1} standard deviation), and δv_i is the measurement uncertainty.

We draw from our posterior with the *emcee* Markov Chain Monte Carlo (MCMC) ensemble sampler (Foreman-Mackey et al. 2013). We run our sampler with 128 walkers for 2000 iterations, rejecting the first 1500 to ensure fully mixed chains. The posterior distributions of v_{sys}, Υ_*, and distance closely match those of the associated prior distributions. For the inference with the SHMR-informed prior, the posterior distribution of the star-cluster system R_e is slightly lower (with median of 26″). The weak-prior model prefers a slightly tangential orbital anisotropy, although consistent with isotropy, while the posterior anisotropy in the SHMR-prior model matches the prior.

4. Halo Mass Inferences

Before discussing the best-fitting results, in Figure 1 we present a comparison between the data and a simple model with a cuspy NFW halo that follows the mean SHMR, assuming isotropic orbits. The individual star-cluster velocity measurements (absolute value relative to v_{sys}) versus galactocentric radius are shown along with a model line-of-sight σ profile (dashed green curve). It is clear that this is not a favorable model: ∼3 of the observed velocities should lie above the curve, which has a spatially averaged $\sigma \sim 36$ km s^{-1}, compared to an observed $\sigma \sim$ 5–10 km s^{-1}.

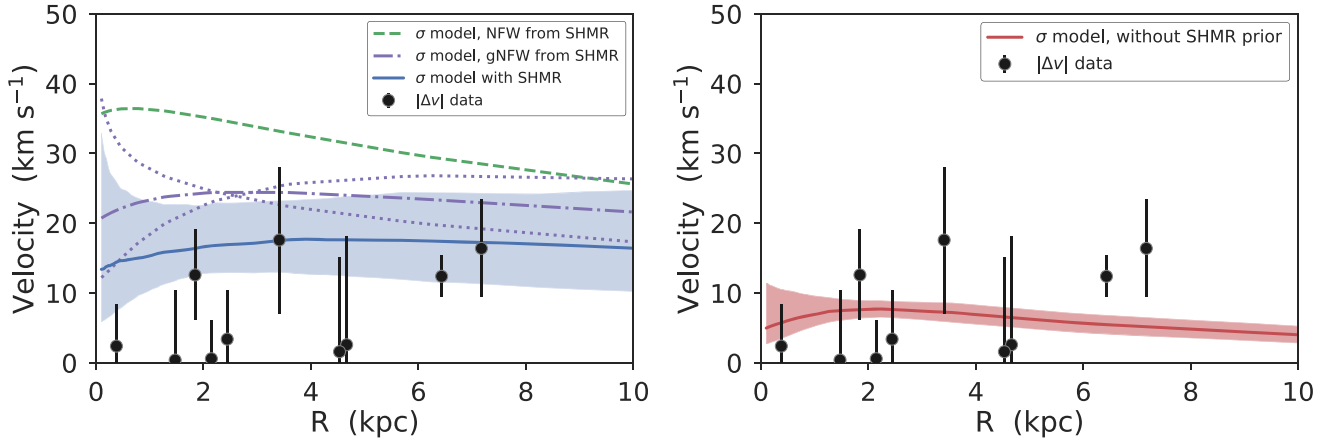

Figure 1. DF2 observed star-cluster velocity offsets (points with error-bars), compared with the posterior predictive distribution of the velocity dispersion profiles associated with the star+halo model fit with freely varying anisotropy and R_e. The shaded regions give the inner 68% of samples. Left panel: the dashed green curve shows an isotropic model with a standard DM halo ($\gamma = 1$ cusp) and halo mass fixed to the SHMR mean. The dotted–dashed purple curve is for a cored DM halo ($\gamma = 0.2$), with fixed halo mass, and isotropic orbits. The dotted purple lines around this curve show the effect of assuming radial (falling profile) and tangential (rising profile) anisotropy. The blue solid curve shows a cored halo with mass informed by a log-normal prior about a standard SHMR. Right panel: the red solid curve shows the model fit with the relaxed prior on halo mass—a model that we see is less in tension with the data than the models with large amounts of DM (left panel).

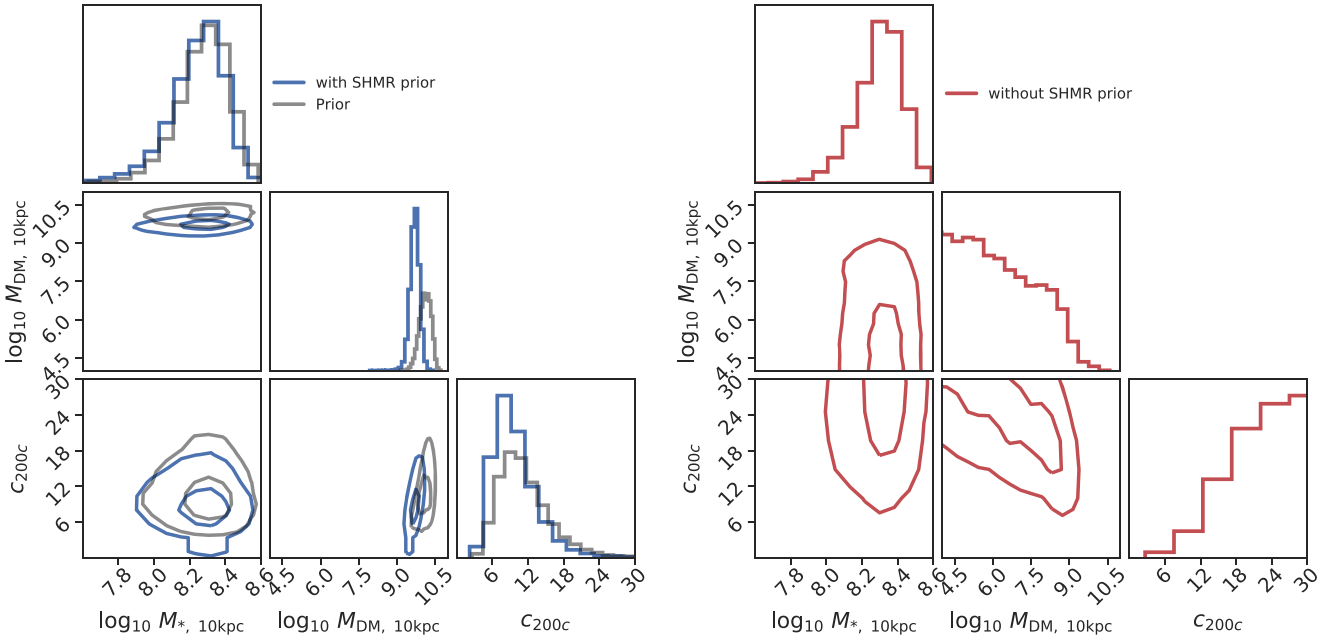

Figure 2. Distributions of select model parameters. The contours showing the covariance between the two parameters are placed at 1- and 2-σ intervals. Masses are in $M_\odot$. Left panel: for the model with the SHMR prior (in blue). The prior distribution is shown in gray. From left to right, the parameters are the stellar mass within 10 kpc, the DM mass within 10 kpc, and the halo concentration. Right panel: the same model parameters but for the model without the SHMR prior. We see that the SHMR prior model largely recovers the prior distribution, though with slightly lower halo mass, while the data-driven model has a halo mass that hits the prior lower boundary.

This is not, however, the only plausible model, as there is scatter in the predicted SHMR and in the halo concentration. Furthermore, UDGs and luminous dwarfs in general are expected to inhabit cored DM halos (Chan et al. 2015; Di Cintio et al. 2017). Allowing for a DM core (dotted–dashed purple curve) reduces the tension with the data somewhat ($\sigma \sim 22$ km s^{-1}). Introducing scatter in the SHMR and the MCR as discussed in Section 3, we present the best "standard" model from our MCMC fitting, including a freely varying orbital anisotropy, as a solid-blue curve with uncertainty envelope in Figure 1. This model dispersion profile is fairly constant with spatially averaged $\sigma = 17^{+6}_{-4}$ km s^{-1} and appears more reasonably close to the data, although it is still in tension with the many observed near-zero relative velocities. The posteriors on some key model parameters are: $\beta = 0.0^{+0.7}_{-2.5}$, $\log_{10} M_{200c}/M_\odot = 10.7^{+0.2}_{-0.3}$, $c_{200c} = 9^{+4}_{-3}$ (implying $r_s = 8^{+4}_{-3}$ kpc), and $\gamma = 0.2^{+0.3}_{-0.2}$, although we note that the samples of γ hit the prior boundary at 0. This is a model solution with a normal halo and concentration (consistent with the priors: see Figure 2, left panel) but a large central density core—strongly disfavoring the NFW model.

We next consider a model that allows for deviation from the standard SHMR, along with a free central DM slope, while still imposing the standard prior on halo mass versus concentration. We find that the DM halo all but disappears, with $M_{200c} < 1.2 \times 10^8\, M_\odot$ ($M_{DM}/M_* < 0.6$) at the 90th percentile. The posterior velocity dispersion profile is shown in Figure 1

(right), with an average $\sigma = 7 \pm 1$ km s^{-1}. This model prefers a more tangential $\beta = -1.0^{+1.2}_{-2.7}$.

For a measure of relative predictive accuracy of these two models, we use the Watanabe–Akaike Information Criterion (WAIC), an approximation of cross-validation (Gelman et al. 2013), defined as

$$\mathrm{WAIC} = -2\sum_{i}^{n} \ln \int \mathcal{L}(v_i \mid \theta) p_{\mathrm{post}}(\theta) d\theta + 4\sum_{i}^{n} \mathrm{var}_{\mathrm{post}}[\ln \mathcal{L}(v_i \mid \theta)] \quad (5)$$

where $p_{\mathrm{post}}(\theta)$ is the posterior distribution, $\mathcal{L}(v_i|\theta)$ is the likelihood, and $\mathrm{var}_{\mathrm{post}}$ is the variance over the posterior. The first term measures the predictive accuracy marginalized over the posterior distribution, while the second term penalizes for model complexity by computing an approximation of the effective number of model parameters (analogous to reduced χ^2). We find $\Delta\mathrm{WAIC} = 1.5$ (equivalent to a model odds ratio of $\sim$2), slightly favoring the model without the SHMR prior, although not enough to reject the SHMR model outright.

As a summary of these results, Figure 2 shows the distribution of stellar and dark mass within a three-dimensional aperture of 10 kpc, as well as the halo concentration for these two models. For the SHMR-prior model, the data prefer a lower enclosed dark mass than in the prior, with a shift in the median M_{DM} within 10 kpc from $1.2 \times 10^{10}\ M_\odot$ to $5.1 \times 10^{9}\ M_\odot$. For the weak-priors model, the posterior distribution of $M_{\mathrm{DM}}(<10\ \mathrm{kpc})$ extends all the way to the lower prior boundary ($\sim 10^2\ M_\odot$), with a 90th-percentile upper bound of $1.2 \times 10^{8}\ M_\odot$. Thus, the data prefer a relatively low amount of DM within the region probed.

The more tightly constrained quantity of interest is the *total* dynamical mass within 10 kpc, which is $(2.2^{+0.9}_{-0.6}) \times 10^8 M_\odot$, or dynamical $M/L_V = 1.7^{+0.7}_{-0.5}$. The latter value is remarkably coincident with the independent stellar population estimate for DF2 (Section 2). We conclude that data-driven dynamical modeling of DF2 allows for at most an extremely low-mass DM halo, and suggests that this UDG is comprised purely of stars.

5. Tidal Effects

The models considered in the previous sections were for an isolated dwarf and neglected any influence from the nearby massive elliptical galaxy, NGC 1052. In particular, infall of a satellite into a larger host initiates a process of tidal stripping, first from the outer DM halo, then from the central regions, followed by total disruption. Tidal stripping and heating has been proposed as the dominant mechanism for forming UDGs, which could be considered as exemplars for galaxies undergoing tidal disruption (Carleton et al. 2018). Some previously studied UDGs are clearly in the process of disruption (Merritt et al. 2016), while many others have undisturbed morphologies out to $\sim 4\ R_{\mathrm{e}}$ (Mowla et al. 2017).

vD+18a presented analysis of tidal stripping to constrain the physical separation between DF2 and NGC 1052. Here our aim is to develop a holistic model where the inferred UDG mass distribution is checked for consistency with tidal constraints, propagating uncertainties on viewing angle, satellite mass distribution, and central galaxy mass. In particular, is a no-DM scenario implausible owing to a likelihood of disruption?

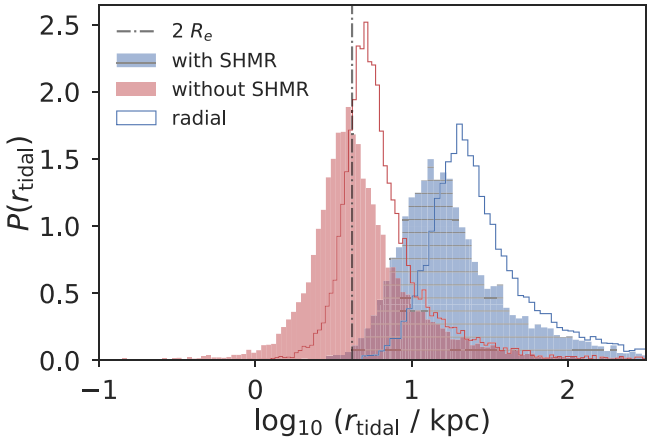

Figure 3. Distribution of DF2 tidal radii inferred for each of the two models. The blue histograms show the limits inferred with a strong SHMR prior, while the red histograms show those for the model without the SHMR prior. The filled histograms show the tidal radius from assuming a circular orbit, while the empty histograms show the same distributions from assuming a radial orbit. The vertical dashed–dotted line shows 2 R_{e} for the starlight. We see that 52% (81%) of the no-SHMR-prior model samples for the circular (radial) orbit are above this lower bound, thus allowing for little/no-DM solutions that do not exhibit tidal disturbances.

We use a simple model for the tidal radius given enclosed masses of satellite and central galaxies:

$$r_{\mathrm{tidal}} = \left(\frac{M_{\mathrm{sat}}(r_{\mathrm{tidal}})}{(\alpha - \gamma_M) M_{\mathrm{cen}}(d)} \right)^{1/3} d, \quad (6)$$

where d is the 3D distance between the two galaxies, γ_M is the local log-slope of the enclosed mass profile of the central galaxy at d, and $\alpha = 2$ if we assume the orbit of the satellite is radial and $\alpha = 3$ if we assume that the orbit is circular (van den Bosch et al. 2018). Without modeling any constraints on the actual orbit of DF2, we compare results assuming either radial or circular orbits for the satellite, assuming that the truth lies somewhere in between these two cases. For our sampled central mass profiles and separation distances, $\gamma_M \sim 1$. DF2 shows no obvious evidence of tidal disturbances, with regular isophotes out to $\approx 2\ R_{\mathrm{e}}$ ($\sim$4 kpc; vD+18a). This provides a tidal constraint that $r_{\mathrm{tidal}} \gtrsim 4$ kpc.

To estimate the central galaxy mass, we use the halo-to-stellar mass relation from Rodríguez-Puebla et al. (2017). For $M_* = 10^{11}\ M_\odot$ (Forbes et al. 2017), we expect $M_{200c} = 4.9 \times 10^{12}\ M_\odot$ with a scatter of 0.25 dex (from inverting the SHMR scatter of 0.15 dex). We then adopt an NFW profile with concentration from the MCR and calculate the enclosed mass at a given radius.

To fold in all the uncertainties together (central mass, satellite mass posterior from the previous inference, and distance), we randomly sample from the underlying parameters, including a uniform distribution of projection angles. We plot the resulting distribution of tidal radii in Figure 3.

For the data-driven model, $r_{\mathrm{tidal}} = 4.3^{+4.7}_{-1.7}$ $(5.7^{+5.09}_{-1.71})$ kpc when assuming a circular (radial) orbit. Thus, there is a large fraction of model-posterior space (52% for circular, 81% for radial) where DF2 can have little/no DM yet be tidally undisturbed out to 4 kpc. We note that the low-velocity star clusters observed out to $\sim$ 7.5 kpc could still be bound even with $r_{\mathrm{tidal}} \sim 4$ kpc, if they have retrograde orbits (Read et al. 2006).

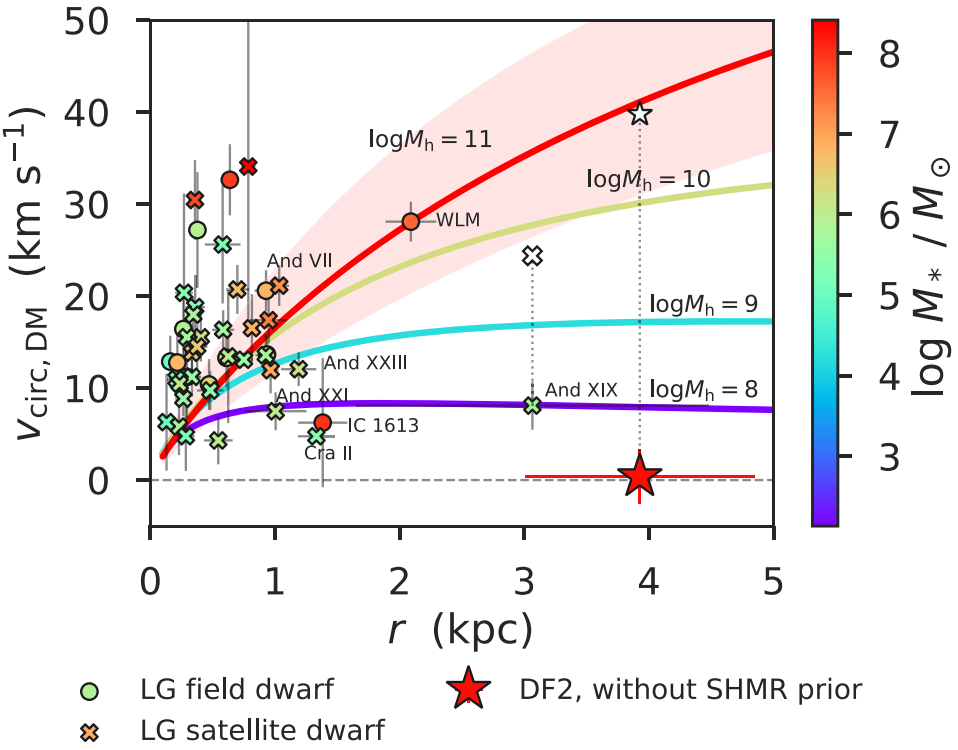

Figure 4. DF2 compared with LG dwarf galaxies. The circles and x's show the circular velocity of the DM component for field and satellite dwarfs, respectively. The points are color coded by stellar mass. The curves show cored ($\gamma = 0.3$) NFW profiles for different halo masses (in $M_\odot$), color coded by the mean expected stellar mass. The posterior predictive value for the data-driven DF2 inference is shown as the star, below $\log M_{200c}/M_\odot = 8$. The open markers with dotted lines for Andromeda XIX and DF2 show the expected DM halos that they would occupy, given their stellar mass. We see that DF2 is an outlier even beyond the extended LG dwarfs in both its size and in mismatch between expected and observed DM halo mass.

Turning to the SHMR-prior model, the dwarf would be naturally much more resistant to tides, and the tidal radius would be farther out (Figure 3). However, the predicted value of $r_{\rm tidal} = 16^{+28}_{-7}$ kpc (or 24^{+33}_{-10} kpc for the radial case) implies that DF2 would still likely have most of its DM stripped away by now, as $M_{\rm DM}(r_{\rm tidal})/M_{200c} \sim 0.2$ ($\sim$0.4).

The latter point leads us to the possibility that DF2 started out with a normal DM halo, but has been tidally eroded, not only by removing the outer parts but also by stripping out much of the central DM prior to disruption of the visible galaxy. Such a solution was studied through N-body simulations by Ogiya (2018), who found that the final dark mass within 10 kpc could be $\sim 10^8\,M_\odot$—which is consistent with our observations (see the red curves in Figure 2). We note, however, two major caveats to this interpretation: (1) there is a small range of orbital parameter space that allows for the necessary degree of stripping; (2) the dynamical time within the UDG is comparable to its orbital period, which may prevent it from relaxing into a visually undisturbed system with cold kinematics.

The difference in predicted tidal radii between the DM and no-DM models motivates looking beyond 4 kpc for tidal features around DF2 to help distinguish between these two scenarios.

6. DF2 in a Wider Context

We have found through Jeans modeling that the observations of cold kinematics in DF2 imply a very low DM content. However, Martin et al. (2018) disputed the unusual nature of this galaxy by noting its similar σ and dynamical M/L to previously studied dwarfs. Here we emphasize that such comparisons neglect the different measurement radii used, and we clarify the position of DF2 in a wider context by constructing a plot relating galaxy stellar masses, halo masses, and sizes (Figure 4).

We take the compilation of LG dwarf galaxies from Fattahi et al. (2018), selecting only galaxies with $M_* > 10^5\,M_\odot$ and updating with sizes from Martin et al. (2016) where available. Taking the dynamical mass within $r_{1/2} \approx 1.3R_{\rm e}$ and subtracting the associated stellar mass, we compute the DM contribution to the circular velocity,

$$v_{\rm circ,\,DM} = \sqrt{\frac{GM_{\rm DM}(<r_{1/2})}{r_{1/2}}}, \tag{7}$$

propagating uncertainties in the distance, size, luminosity, stellar M/L, and velocity dispersion. We color these points in Figure 4 by their stellar mass, with different symbols for field dwarfs versus satellites. We compare these measurements with halo circular velocity profiles for several halo masses, adopting MCR concentrations and $\gamma = 0.3$ cores, while color-coding these profiles by the SHMR-predicted stellar mass. The halo-concentration scatter is illustrated by the red band for the $10^{11}\,M_\odot$ halo.

This figure shows that some dwarfs track cored-halo profiles appropriate to their stellar masses. Others have higher velocities and perhaps cuspy halos (e.g., Spekkens et al. 2005; Oñorbe et al. 2015; Genina et al. 2018). A few have low velocities; as most of these are satellites, they may be examples of ongoing tidal stripping that has depleted their central DM content (Collins et al. 2013; Buck et al. 2018; Fattahi et al. 2018). DF2, however, stands out from all of these galaxies by

having the lowest DM-velocity estimate, despite the much larger measurement radius. Andromeda XIX is closest in σ–$r_{1/2}$ space, but has $\sim$300$\times$ lower stellar mass and thus does not appear as DM-depleted as DF2. IC 1613 has a high stellar mass, but the smaller measurement radius allows for a larger range of halo masses.

We therefore strengthen the conclusion of vD+18a that DF2 is an extreme outlier in the usual dwarf–DM scaling relations. There are then two main possible explanations. One is that the galaxy formed with little or no DM, and the other is that it has been severely stripped of DM. We cannot definitively discriminate between the two scenarios, but in Section 5 we pointed out potentially major flaws in the tidal argument. Furthermore, there is an additional clue that has so far been generally overlooked: the very star-cluster system used to probe the dynamics of DF2 is itself so far unique in the known universe. The clusters are on average far more luminous than in other galaxies including the Milky Way, and they are also unusually extended and elongated (van Dokkum et al. 2018b). The presence of either a normal or a stripped DM halo provides no explanation for this novel observation. On the other hand, if DF2 formed through a rare pathway without DM (e.g., scenarios discussed in vD+18a), then it is more plausible that its star-cluster system would show unusual properties as well.

The peculiar case of DF2 demonstrates the rich yield of information that can be obtained through detailed observations of dwarfs beyond the LG, which will help challenge and refine our understanding of galaxy formation and of the nature of DM.

We thank the anonymous referee for useful suggestions. A.W. thanks Viraj Pandya for helpful discussions. This work was supported by NSF grants AST-1616598 and AST-1616710. A.J.R. is a Research Corporation for Science Advancement Cottrell Scholar.

ORCID iDs

Asher Wasserman https://orcid.org/0000-0003-4235-3595
Aaron J. Romanowsky https://orcid.org/0000-0003-2473-0369
Jean Brodie https://orcid.org/0000-0002-9658-8763
Pieter van Dokkum https://orcid.org/0000-0002-8282-9888
Charlie Conroy https://orcid.org/0000-0002-1590-8551
Roberto Abraham https://orcid.org/0000-0002-4542-921X
Yotam Cohen https://orcid.org/0000-0001-5487-2494
Shany Danieli https://orcid.org/0000-0002-1841-2252

References

Aaronson, M. 1983, ApJL, 266, L11
Adams, J. J., Simon, J. D., Fabricius, M. H., et al. 2014, ApJ, 789, 63
Amorisco, N. C., Monachesi, A., Agnello, A., & White, S. D. M. 2018, MNRAS, 475, 4235
Beasley, M. A., Romanowsky, A. J., Pota, V., et al. 2016, ApJL, 819, L20
Brown, W. R., Geller, M. J., Kenyon, S. J., & Kurtz, M. J. 2007, ApJ, 666, 231
Buck, T., Macciò, A. V., Dutton, A. A., Obreja, A., & Frings, J. 2018, arXiv:1804.04667
Carleton, T., Errani, R., Cooper, M., Kaplinghat, M., & Peñarrubia, J. 2018, arXiv:1805.06896
Chan, T. K., Kereš, D., Oñorbe, J., et al. 2015, MNRAS, 454, 2981
Chapman, S. C., Ibata, R., Lewis, G. F., et al. 2005, ApJL, 632, L87
Cohen, Y., van Dokkum, P., Danieli, S., et al. 2018, arXiv:1807.06016
Collins, M. L. M., Chapman, S. C., Rich, R. M., et al. 2013, ApJ, 768, 172
Di Cintio, A., Brook, C. B., Dutton, A. A., et al. 2017, MNRAS, 466, L1
Diemer, B. 2017, arXiv:1712.04512
Diemer, B., & Kravtsov, A. V. 2015, ApJ, 799, 108
Fattahi, A., Navarro, J. F., Frenk, C. S., et al. 2018, MNRAS, 476, 3816
Forbes, D. A. 2017, MNRAS, 472, L104
Forbes, D. A., Sinpetru, L., Savorgnan, G., et al. 2017, MNRAS, 464, 4611
Foreman-Mackey, D., Hogg, D. W., Lang, D., & Goodman, J. 2013, PASP, 125, 306
Fosbury, R. A. E., Mebold, U., Goss, W. M., & Dopita, M. A. 1978, MNRAS, 183, 549
Garrison-Kimmel, S., Bullock, J. S., Boylan-Kolchin, M., & Bardwell, E. 2017, MNRAS, 464, 3108
Gelman, A., Hwang, J., & Vehtari, A. 2013, arXiv:1307.5928
Genina, A., Benítez-Llambay, A., Frenk, C. S., et al. 2018, MNRAS, 474, 1398
Greco, J. P., Greene, J. E., Price-Whelan, A. M., et al. 2018, PASJ, 70, S19
Karachentsev, I. D., Karachentseva, V. E., Suchkov, A. A., & Grebel, E. K. 2000, A&AS, 145, 415
Kleyna, J. T., Wilkinson, M. I., Evans, N. W., & Gilmore, G. 2005, ApJL, 630, L141
Koposov, S. E., Casey, A. R., Belokurov, V., et al. 2015, ApJ, 811, 62
Laporte, C. F. P., Agnello, A., & Navarro, J. F. 2018, arXiv:1804.04139
Lim, S., Peng, E. W., Cote, P., et al. 2018, arXiv:1806.05425
Martin, N. F., Collins, M. L. M., Longeard, N., & Tollerud, E. 2018, ApJL, 859, L5
Martin, N. F., Ibata, R. A., Lewis, G. F., et al. 2016, ApJ, 833, 167
Martínez-Delgado, D., Läsker, R., Sharina, M., et al. 2016, AJ, 151, 96
Merritt, A., van Dokkum, P., Danieli, S., et al. 2016, ApJ, 833, 168
Moster, B. P., Naab, T., & White, S. D. M. 2013, MNRAS, 428, 3121
Mowla, L., van Dokkum, P., Merritt, A., et al. 2017, ApJ, 851, 27
Munshi, F., Brooks, A. M., Applebaum, E., et al. 2017, arXiv:1705.06286
Navarro, J. F., Frenk, C. S., & White, S. D. M. 1997, ApJ, 490, 493
Ogiya, G. 2018, MNRAS, 480, L106
Oh, S.-H., de Blok, W. J. G., Brinks, E., Walter, F., & Kennicutt, R. C., Jr. 2011, AJ, 141, 193
Oñorbe, J., Boylan-Kolchin, M., Bullock, J. S., et al. 2015, MNRAS, 454, 2092
Pandya, V., Romanowsky, A. J., Laine, S., et al. 2018, ApJ, 858, 29
Peng, E. W., & Lim, S. 2016, ApJL, 822, L31
Pineda, J. C. B., Hayward, C. C., Springel, V., & Mendes de Oliveira, C. 2017, MNRAS, 466, 63
Read, J. I., Wilkinson, M. I., Evans, N. W., Gilmore, G., & Kleyna, J. T. 2006, MNRAS, 366, 429
Rodríguez-Puebla, A., Primack, J. R., Avila-Reese, V., & Faber, S. M. 2017, MNRAS, 470, 651
Smercina, A., Bell, E. F., Price, P. A., et al. 2018, arXiv:1807.03779
Spekkens, K., Giovanelli, R., & Haynes, M. P. 2005, AJ, 129, 2119
Toloba, E., Lim, S., Peng, E., et al. 2018, ApJL, 856, L31
Trujillo, I., Beasley, M. A., Borlaff, A., et al. 2018, arXiv:1806.10141
van den Bosch, F. C., Ogiya, G., Hahn, O., & Burkert, A. 2018, MNRAS, 474, 3043
van der Burg, R. F. J., Hoekstra, H., Muzzin, A., et al. 2017, A&A, 607, A79
van Dokkum, P., Abraham, R., Brodie, J., et al. 2016, ApJL, 828, L6
van Dokkum, P., Cohen, Y., Danieli, S., et al. 2018a, RNAAS, 2, 54
van Dokkum, P., Cohen, Y., Danieli, S., et al. 2018b, ApJL, 856, L30
van Dokkum, P., Conroy, C., Villaume, A., Brodie, J., & Romanowsky, A. J. 2017, ApJ, 841, 68
van Dokkum, P., Danieli, S., Cohen, Y., et al. 2018c, Natur, 555, 629
van Dokkum, P. G., Abraham, R., Merritt, A., et al. 2015, ApJL, 798, L45
van Dokkum, P. G., Danieli, S., Cohen, Y., & Conroy, C. 2018d, arXiv:1807.06025
Wasserman, A., Romanowsky, A. J., Brodie, J., et al. 2018, ApJ, in press (arXiv:1712.01229)
Yagi, M., Koda, J., Komiyama, Y., & Yamanoi, H. 2016, ApJS, 225, 11